Multifunctional and Recollectable Carbon Nanotube Ponytails for Water Purification

Haitao Wang,[†,§] Hanyu Ma,[†,§] Wen Zheng,[‡] Dingding An,*[,‡] and Chongzheng Na*[,†]

[†]Department of Civil and Environmental Engineering and Earth Sciences, University of Notre Dame, Notre Dame, Indiana 46556, United States

[‡]Department of Microbiology and Immunobiology, Harvard Medical School, Boston, Massachusetts 02115, United States

Ⓢ Supporting Information

ABSTRACT: Carbon nanotubes (CNTs) are promising nanomaterials that have the potential to revolutionize water treatment practices in the future. The direct use of unbounded CNTs, however, poses health risks to humans and ecosystems because they are difficult to separate from treated water. Here, we report the design and synthesis of carbon nanotube ponytails (CNPs) by integrating CNTs into micrometer-sized colloidal particles, which greatly improves the effectiveness of post-treatment separation using gravitational sedimentation, magnetic attraction, and membrane filtration. We further demonstrate that CNPs can effectively perform major treatment tasks including adsorption, disinfection, and catalysis. Using model pollutants such as methylene blue, *Escherichia coli*, and *p*-nitrophenol, we show that all the surfaces of individual CNTs in CNPs are accessible during water treatment. Our results suggest that the rational design of hierarchical structures represents a feasible approach to develop nanomaterials for engineering applications such as water and wastewater treatment.

KEYWORDS: carbon nanotube array, composite without polymeric binder, palladium nanoparticles, layered double hydroxide, layered double oxide, industrial wastewater, pathogenic microorganism

INTRODUCTION

Carbon-based materials are widely used in water and gas purification as well as food processing and drug production.[1] The most common carbon-based material is activated carbon produced by pyrolysis of precursors such as nutshell, coconut husk, and peat. Activated carbon often takes the form of porous colloidal particles, which consist of tortuous channels aligned with nanometer-sized graphitic nanocrystals. In 2011, the worldwide consumption of activated carbon has reached 1.2 million metric tons with sales worth $2 billion U.S. dollars (comparable to the gross domestic product of a country like Maldives).[2] The global market of activated carbon is predicted to grow at a compound annual rate of 10% in the next five years.[3] Among all applications, the application in municipal and industrial water treatment dominates the use of activated carbon.[2]

Carbon nanotubes (CNTs) have attracted increasing attention as potential substitutes for activated carbon. Many believe that applications of nanomaterials such as CNTs may lead to game-changing transformation of water treatment technologies in the future,[4−6] which will particularly benefit people in impoverished countries that do not currently have water treatment infrastructures.[7,8] CNTs are made of rolls of carbon sheets that have diameters in the nanometer range but lengths varying from tens of nanometers up to a few centimeters.[9] Depending on the number of carbon rolls, carbon nanotubes are categorized as single-walled, few-walled, and multiwalled CNTs. CNTs can provide a wide range of functions in water treatment including adsorbing chemical pollutants,[10−14] disinfecting pathogenic microorganisms,[15] and supporting catalysts for contaminant degradation.[16] Compared to activated carbon whose microscopic pores are often blocked during adsorption, CNTs' open structure offers easy, undisrupted access to reactive sites located on nanotubes' outer surface. Although activated carbon often has a much higher specific surface area (500−1000 $m^2 g^{−1}$) than CNTs (433 $m^2 g^{−1}$ or less for CNTs with more than one wall), CNTs frequently exhibit higher capacity and faster kinetics in sorption than activated carbon, which have been attributed to the rapid transfer of contaminants from water to CNT surfaces due to CNTs' open structure.[17−19] Furthermore, CNTs' open structure also provides convenience for modifying surface chemistry. The sp^2-hybridized C atoms in CNTs can be readily converted to sp^3-hybridized C atoms, which can host surface functionalities such as hydroxyl (−OH) and carboxyl (−COOH) groups to improve adsorption selectivity.

In spite of CNTs' exciting properties, the direct use of CNTs in water treatment faces the challenge of recollecting them after

treatment. Conventionally, powdered activated carbon (PAC) particles are collected by gravitational sedimentation, filtration, or coagulation after use.[20] Different from PAC, none of the conventional techniques is expected to work well for CNTs. CNTs do not settle well under gravity due to their small sizes. With their small sizes, CNTs can easily cause clogging of filtration membranes and packed beds. Although coagulation can separate CNTs, mixing them with coagulants makes it difficult to recycle, regenerate, and reuse the expensive material (ca. $100 per kg for CNTs vs $1.5 per kg for activated carbon). CNTs left in treated water not only incur costs for replenishment but also cause concerns for potential adverse effects on human health and the health of ecosystems.[21−25]

A potential solution to CNTs' recollection challenge is to attach CNTs on colloidal particles made of supporting materials such as aluminum oxide[26−28] and silicon carbide.[29] Although attaching CNTs on large, heavy particles improves collectability, the final composite product only has CNTs as a minor component in terms of both mass and volume. Transporting nonreactive supports with a large mass over distance and dispersing them in water waste energy. Placing the supports with a large volume in packed beds wastes space. To develop colloidal CNT composites for water treatment, an imperative challenge is to design a hierarchical structure that has not only an increased overall size but also high CNT mass and volume fractions. To our knowledge, there is no report in the literature that has described any design strategy to achieve these seemingly contradictory goals.

Here, we report a strategy to produce CNT colloidal particles that are hundreds of micrometers in size and have CNT mass and volume fractions of nearly 100%. We designate these particles as carbon nanotube ponytails (CNPs). CNPs are synthesized by growing CNT arrays of hundreds of micrometers in length on nanometer-thin mineral discs. Like individual CNTs, CNPs can be synthesized using thermal chemical vapor deposition (CVD). Different from unbounded CNTs, however, CNPs can be separated more effectively using common techniques such as gravitational sedimentation, magnetic attraction, and membrane filtration. We further show that CNPs can perform all major water treatment tasks effectively as sorbent, disinfectant, and catalyst support. Laboratory evaluations of treatment performance have provided evidence that the structural integration of CNTs into CNPs does not sacrifice the accessibility of CNTs' surface; therefore, one of the most important advantages of CNTs over conventional materials such as activated carbon and clay particles is preserved.[30,31]

RESULTS AND DISCUSSION

Synthesis and Characterization of Carbon Nanotube Ponytails. We synthesized carbon nanotube ponytails using a three-step procedure,[32−34] as outlined in Figure 1. First, layered double hydroxide (LDH; Figure S1a, Supporting Information) discs of a few micrometers in size and approximately 50 nm in thickness are prepared by coprecipitating aluminum, magnesium, and cobalt cations with hydroxide and carbonate anions (produced by the decomposition of urea).[35] Second, LDH discs are transformed to layered double oxide (LDO; Figure S1b, Supporting Information) by dehydration and decarbonation at 800 °C in argon. The treatment produces cobalt oxide (CoO) nanoparticles through phase separation. Third, CoO is reduced to Co by H₂ and then entangled CNT arrays are grown using CVD on both sides of LDO discs at 800 °C using ethanol as
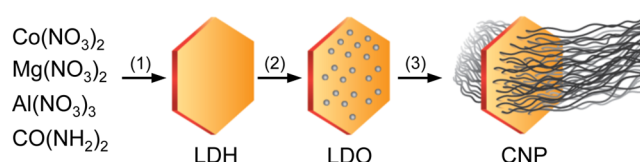
Figure 1. Synthesis of carbon nanotube ponytails: (1) formation of layered double hydroxide (LDH) discs, (2) transformation of LDH to layered double oxide (LDO) discs, and (3) growth of carbon nanotube arrays on LDO.

the carbon source. This procedure typically yields ca. 70 g of CNTs for each gram of Co catalyst (cf. Figure S2, Supporting Information).

The physical properties of a typical CNP sample are shown in Figure 2. As revealed by scanning electron microscopy
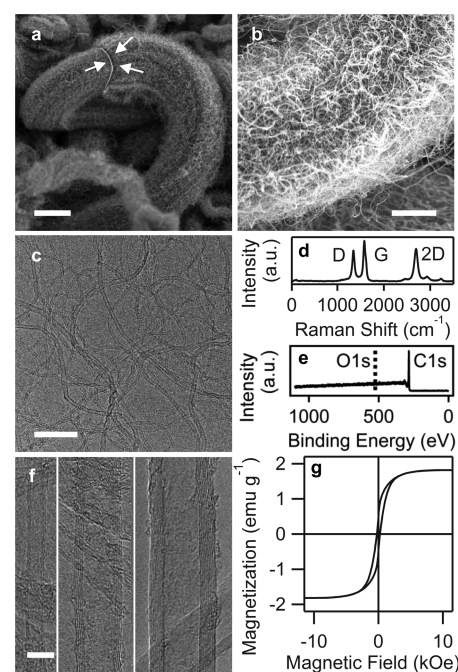
Figure 2. Carbon nanotube ponytails. (a, b) Scanning electron micrographs (layered double oxide discs marked by arrows). (c, f) Transmission electron micrographs of CNTs in CNPs. (d) Raman spectrum. (e) X-ray photoelectron spectrum. (g) Magnetic loop of CNPs. Scale bars: a, 3 μm; b, 1 μm; c, 100 nm; f, 5 nm.

(SEM), a dry CNP particle has a flexible cylindrical structure with a diameter of a few micrometers and a length of tens of micrometers (Figure 2a). Each CNP particle consists of two arrays of entangled CNTs anchored on a thin LDO disc (marked by arrows), which has a negligible contribution to the overall mass and volume. A close view shows that the CNT arrays are porous and consist of curvy nanotubes (Figure 2b). Transmission electron microscopy (TEM) shows that individual CNTs have a relatively narrow distribution of diameters (Figure 2c). Raman spectroscopy shows that CNTs contain defects giving a D/G ratio of 0.8 (Figure 2d). Using the empirical relationship $L_a = 8.28/(I_D/I_G)$,[36,37] we estimate the size of in-plane graphene crystallites at $L_a = 10.4$ nm, suggesting the presence of one defect site every 10.4 nm on average. Although oxidation can form defects on CNT surfaces,[38] the defects seen here are likely not formed by oxidation because little oxygen is found by X-ray photoelectron spectroscopy

(Figure 2e). The lack of surface oxygen indicates that CNPs are hydrophobic. High-resolution TEM further reveals that the outer diameter and wall number of individual CNTs, which can be controlled during synthesis, vary from 4 to 9 nm and from 2 to 10, respectively (Figure 2f). Another important property of CNPs is that they are magnetic with a saturation magnetization of 1.8 emu g^{-1} because of the presence of cobalt oxide nanoparticles in LDO (Figure 2g). CNPs' saturation magnetization is 50 times smaller than the value for magnetite.[39] It is sufficiently weak to prevent CNPs from aggregating under self-attraction but strong enough to be utilized for separation (see below).

Our synthesis procedure allows the control of CNPs' morphology such as LDH size, CNT length, CNT diameter, and CNT wall number by varying synthesis conditions (Figure S2, Supporting Information, and the accompanying text). The changes of these parameters lead to the variation of the specific surface area (SSA) of CNPs, which is characterized by nitrogen physisorption. As shown in Figure 3a, a typical sorption isotherm reveals that the amount of adsorbed N$_2$ by each gram of CNPs, S, increases slowly at low N$_2$ pressures for $P/P_0 < 0.6$, suggesting a weak N$_2$–CNT interaction. As P/P_0 becomes greater than 0.8, S increases rapidly with increasing P/P_0, suggesting an improved adsorption due to a strong N$_2$–N$_2$ interaction. Moreover, the lack of hysteresis between the

desorption and adsorption isotherms indicates little resistance for mass transfer. These characteristics are consistent with a type III behavior for a highly porous material.[40] Indeed, the pore size distribution calculated by the non-local density functional theory reveals a broad range of pores with diameters spanning from 2 to 100 nm, as shown in Figure 3b. We assign the peak at 2.9($\pm$1.3) nm to the adsorption of N$_2$ by the N$_2$–CNT interaction around individual CNTs, which is consistent with the CNT diameter of 4–7 nm calculated from nanotube dimensions. We assign the broad band between 4.5 and 100 nm to the adsorption of N$_2$ by the N$_2$–N$_2$ interaction and accommodated by CNPs' porous structure.

We estimate the SSA of CNPs, S_{BET}, using the Brunauer–Emmett–Teller (BET) equation:[41] $[S(P_0/P - 1)]^{-1} = (1 - 1/c)S_{BET}^{-1}(P/P_0) + S_{BET}^{-1}c^{-1}$, where c is the BET constant. Using the monolayer portions of the adsorption and desorption curves ($P/P_0 < 0.5$), we obtain 365($\pm$10) m^2 g^{-1} through least-squares regression. Similarly, the SSAs are obtained for three other CNP samples prepared under different synthesis conditions. The values of S_{BET} range from 200 to 500 m^2 g^{-1}, comparable to the typical surface areas of activated carbon.[20] As shown in Figure 3c, these values are compared to the SSAs computed from the physical dimensions of CNTs in each sample: $S_{cal} = 4d^{-1}\rho^{-1}$, where d is the CNT diameter and ρ is the CNT density.[42] Values of S_{BET} and S_{cal} agree well with each other, as evident from the linear correlation with a slope of unity, suggesting that CNPs have an open structure when they are dry.

Separation of Carbon Nanotube Ponytails. To evaluate CNPs' performance in separation, we selected the CNP sample with a LDH size of 2.0($\pm$0.2) μm, a CNT length of 60($\pm$25) μm, a CNT diameter of 6.0($\pm$1.4) nm, a CNT wall number of 4($\pm$1), and S_{BET} = 365($\pm$10) m^2 g^{-1} (marked by the red circle in Figure 3). This sample has a CNT density of ρ = 3.04$[n/d - (0.34\sum_{i=0}^{n-1} i)/d^2]$ = 1.9($\pm$0.5) g cm^{-3}.[43] Quantitative assessments of CNPs' behavior in the common separation processes, including (a) gravitational sedimentation, (b) magnetic separation, and (c) membrane filtration, are discussed as follows.

Gravitational sedimentation is widely used in both large-scale facilities and personal devices for water purification.[44] As shown in Figure 4a, CNPs (colored in green) continuously settle from an aqueous suspension with an initial concentration of X_0 = 35 mg L^{-1}, which is comparable to the use of activated carbon in water treatment.[20] After 60 min, the originally opaque CNP suspension has become clear. In comparison, unbounded CNTs (colored in red) with similar surface hydrophobicity do not settle well within the same period of time, as evident from the CNT suspension's opacity. Two settling regimes are revealed by quantitative analyses of changes of carbon concentration X with time t. In regime I where $X > 15$ mg L^{-1}, CNPs and CNTs behave similarly because both of them settle as aggregates.[45] In regime II where aggregates reduce to individual particles as X decreases, CNPs settle faster than CNTs because CNPs are bigger. The settling processes in both regimes conform to the sedimentation model: $X = X_0e^{-(v/h)t}$,[46] where v is the settling velocity and h = 1.2($\pm$0.1) cm is the height of the suspension. Least-squares regressions give v_I = 10.6($\pm$0.6) cm h^{-1} for both CNTs and CNPs but v_{II}(CNPs) = 2.2($\pm$0.3) cm h^{-1} and v_{II}(CNTs) = 0.14($\pm$0.03) cm h^{-1}. For a personal water purification device (e.g., a water bottle) with a settling height of 2 cm (bottle placed horizontally), 95% of CNPs can be settled out in 2.3 h. For sedimentation tanks used
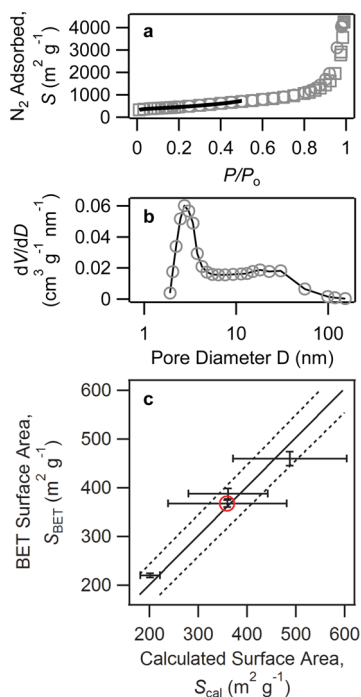
Figure 3. Specific surface area of carbon nanotube ponytails (CNPs). (a) Representative adsorption (squares) and desorption (circles) of N$_2$ at 77 K expressed in the total surface area of N$_2$/g of carbon nanotube ponytails (CNPs) vs the normalized N$_2$ pressure. The solid curve is a least-squares fit to the BET equation (see text for details). (b) Pore size distribution calculated by the non-local density functional theory. (c) Correlation of the specific surface area obtained by fitting N$_2$ adsorption to the BET equation with that computed from the morphological dimensions of CNPs (see text for details). The solid line is a least-squares linear regression (S_{BET} = 1.01($\pm$0.03)S_{cal}, R^2 = 0.99). Dashed lines are the confidence intervals corresponding to one standard deviation. The red circle marks the sample used for further evaluation of separation and water treatment.
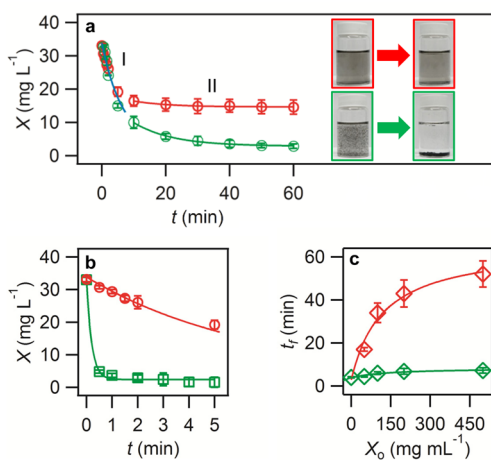
Figure 4. Separation of CNPs (green), compared to unbounded CNTs (red), from clean water by (a) gravitational sedimentation (circles), (b) magnetic attraction (squares), and (c) membrane filtration (diamonds). Curves are least-squares regressions of different separation models (see text for details).

for industrial or municipal water treatment that have depths of meters but residence times of merely a couple of hours,[44] gravitational sedimentation is no longer practical for CNP separation (of course, also impractical for CNT separation).

Magnetic nanomaterials such as CNPs can be separated using an external magnetic field.[39] Magnetic separation of CNPs can be designed to be much faster than gravitational separation by using a magnetic field that induces an attractive force much stronger than gravity. As shown in Figure 4b, a magnetic field with an average strength of 4 kOe can separate more than 95% CNPs within less than 5 min (squares), which is much faster than separation under gravitational sedimentation (circles). Using $X = X_0 e^{-(v/D)t}$,[46] where $D = 2.8$ cm is the diameter of the vial containing the CNP suspension (magnet placed on the side), the separation velocity is estimated at $v_m = 5.8(\pm 1.3)$ m h^{-1}. In a typical sedimentation tank with a depth of 2 m and a residence time of 2 h,[44] 99.7% removal of CNPs can be accomplished under v_m. In addition to the rapid separation, the use of magnetic force can also avoid the trapping of CNPs at the water−air interface by surface tension under gravity (black dots on top of the water table in the lower right inset in Figure 4a).

Membrane filtration is another option for CNT separation that is often used in laboratory experiments.[47] Figure 4c shows the time required to pass 50 mL of an aqueous suspension of CNPs or CNTs through a 0.8 μm membrane under the pulling of a vacuum. As the initial carbon concentration X_0 increases, the filtration time t_f increases with decreasing flow rate ($Q \propto 1/t_f$) for both CNPs (green) and CNTs (red). The decrease of flow rate is attributable to the formation of a porous film of CNTs or CNPs on top of the filtration membrane. The main determinant of flow reduction is the porosity of the film. The relationship between t_f and X can be modeled with $t_\infty - t_f = \alpha(X_0 + X_m)^{-1}$, where t_∞ is the time for the porosity of carbon film to reach a steady-state value, X_m is the equivalent carbon concentration of the filtration membrane, and α represents the hydraulic resistance of the porous film.[48] According to experimental data, $\alpha_{CNTs}/\alpha_{CNPs} = 12.5$, suggesting that CNPs form more loosely packed films than CNTs and thus can save energy and reduce clogging in filtration.

Carbon Nanotube Ponytails in Water Treatment. The effectiveness of CNPs as sorbent, disinfectant, and catalyst support used in water treatment processes is demonstrated in this section. The demonstration was performed using the same CNP sample that had been used for the evaluation of CNP separation.

CNPs' adsorption capability was tested using methylene blue (MB) as a model pollutant.[49,50] As shown in Figure 5a and b,
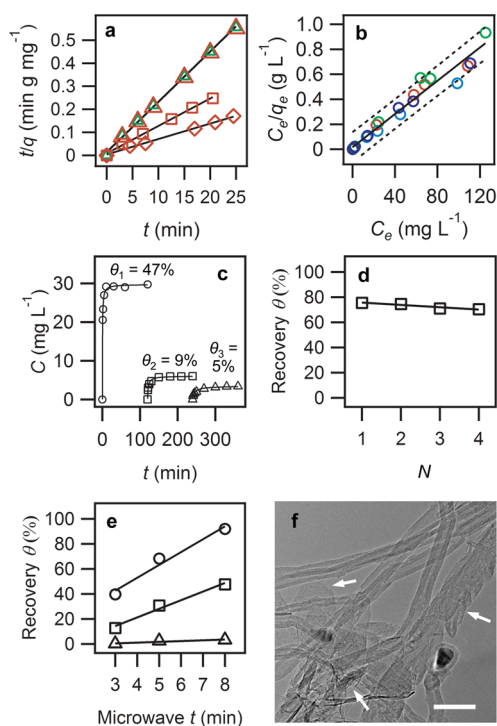
Figure 5. Adsorption of methylene blue by carbon nanotube ponytails. (a) Kinetics of methylene blue (MB) adsorption. Symbols: triangles, $C_0 = 30$ mg L^{-1}; squares, $C_0 = 60$ mg L^{-1}; diamonds, $C_0 = 200$ mg L^{-1}. (b) Adsorption isotherm of methylene blue measured after 4 h of incubation. Solid lines are linear regressions. Dashed lines are 95% confidence intervals. Symbols: cyan, pH 4; crimson, pH 6; green, pH 8; purple, pH 10. (c) Desorption of 10 mg of CNPs using three consecutive cycles of 15 mL ethanol wash. Symbols: circles, first cycle; squares, second cycle; triangles, third cycle. (d) Recovery of CNPs' occupied sites in five adsorption−desorption cycles. (e) Recovery of CNPs' occupied sites using microwave heating. Symbols: circles, first cycle; squares, second cycle; triangles, third cycle. (f) Transmission electron micrograph of microwave-irradiated used CNPs. Arrows: graphitic sheets formed by adsorbed MB. Scale bar: 50 nm.

both kinetics and equilibrium of MB adsorption by CNPs conform to the classical Langmuir model. The kinetic study was performed at two different pH conditions and three different initial concentrations. Results can all be fitted to the linearized model:[51] $t/q = t/q_e + 1/(k_a q_e^2)$, where $q = (C_0 - C)/X$ is the amount of MB adsorbed by CNPs at time t, $C_0 = 30$, 60, or 200 mg L^{-1} is the initial MB concentration, C is the residual MB concentration at t, $X = 0.67$ g L^{-1} is the dose of CNPs, q_e is the equilibrium value of q ($t \rightarrow \infty$), and k_a is the adsorption rate constant. Adsorption is insensitive to pH because MB is always a monovalent cation in the normal pH range.[12,52] As shown in Figure 5a, least-squares regressions reveal that, for $C_0 < 30$ mg L^{-1}, adsorption approaches equilibrium in less than an hour (Table S1, Supporting Information). As shown in Figure 5b, results obtained from adsorption experiments performed for 4

h at different pH, C_0, and X values conform to the Langmuir isotherm:[53] $C_e/q_e = C_e/q_{max} + 1/(Kq_{max})$, where C_e is the residual MB concentration at equilibrium and q_{max} is the adsorption capacity. Regression gives $q_{max} = 150(\pm 9)$ mg g^{-1} (Table S2, Supporting Information). Using q_{max}, the specific surface area of CNPs is computed from $S_{MB} = N_A \tau q_{max}/M = 367(\pm 22)$ m^2 g^{-1}, where $\tau = 1.30$ nm^2 is the surface area that a MB molecule occupies,[54−57] $M = 320$ g mol^{-1} is MB's molecular weight, and $N_A = 6.02 \times 10^{23}$ mol^{-1} is Avogadro's number. This equation is valid because MB forms a monolayer on the CNT surface via $\pi-\pi$ interaction.[12,52] S_{MB} agrees well with the values of S_{cal} and S_{BET}, indicating that all the surfaces of individual CNTs in CNPs are still accessible for adsorbing pollutants in water.

To assess the possibility of removing MB from CNPs by solvent wash, a multicycle process using ethanol is first evaluated.[49,58] As shown in Figure 5c, used CNPs with 65% surface covered (i.e., $q_e = 65\% q_{max}$) are washed in three cycles with each using 15 mL of ethanol. In each cycle, the MB concentration in ethanol, C, increases from 0 and then reaches a plateau after a period of time, suggesting that the removal has reached equilibrium and fresh ethanol is necessary at the end of each cycle. After the washed CNPs are collected from ethanol by magnetic separation, they are mixed with another 15 mL of fresh ethanol and the removal process is repeated. For all of the cycles, the removal kinetics is found to conform to the Langmuir model (Table S3, Supporting Information): $(t - t_{0,n})/C = (t - t_{0,n})/C_{e,n} + 1/(k_{d,n}C_{e,n}^2)$, where t is time, $t_{0,n}$ is the starting time for the nth wash, C is the MB concentration in ethanol, $C_{e,n}$ is the equilibrium MB concentration, and $k_{d,n}$ is the desorption rate constant. The percentage of freed sites by washing is computed as $\theta = C_{e,n}X/q_{0,n}$, where $q_{0,n}$ is the initial concentration of MB on CNPs. For the first wash, $q_{0,1}$ is equal to $q_e = 98$ mg g^{-1} (65% q_{max}, obtained from the adsorption experiment); for subsequent washes, $q_{0,n-1} = q_{0,n} - C_{e,n}X$. As shown in Figure 5c, θ diminishes as n increases, indicating a typical behavior of desorption equilibrium as the mechanism of MB removal in ethanol wash. After CNPs are regenerated by 10 wash cycles, $\theta = 75\%$ is confirmed by readsorbing MB, as shown in Figure 5d ($N = 1$). When the CNPs are used repeatedly after being administered to the adsorption−desorption ($n = 10$) reuse cycle, θ decreases slightly after each cycle (ca. 2% reduction; Table S4, Supporting Information), suggesting that a small fraction of CNTs are bundled together under the attraction of MB. Obviously, a common solvent such as ethanol is unsuitable for regenerating MB-laden CNPs because of the strong MB−CNT affinity and the large quantity of ethanol needed as a result.

An alternative approach of regeneration is thermal treatment, which is regularly performed for used activated carbon. Because CNTs are good adsorbents of microwaves, thermal treatment may be performed using microwave irradiation.[59] As shown in Figure 5e, 92% of the adsorption capacity is restored after used CNPs (65% covered with MB) are irradiated in a kitchen microwave oven for 8 min under maximum power. As the number of regeneration-and-reuse cycles increases, the restored capacity starts to decrease. The decrease can be attributed to the formation of graphitic sheets by adsorbed MB, as shown in Figure 5f (marked by arrows), which destruct the organized porous structure of CNPs. The microwave-assisted thermal treatment may be further optimized to evaporate adsorbed MB without graphitizing MB, which is beyond the scope of the present study.

Through sorption, CNPs can be used to remove pathogenic microorganisms from water and thus achieve disinfection without using potentially harmful chemicals.[60] CNPs' potential as a disinfectant was evaluated using bacterium *Escherichia coli* DH5α (*E. coli*) as a model pathogen. The removal of *E. coli* from water was measured by the reduction in colony forming units (CFUs) after 1 h of contact with CNPs. As shown in Figure 6a, the removal of *E. coli* increases with the increase of
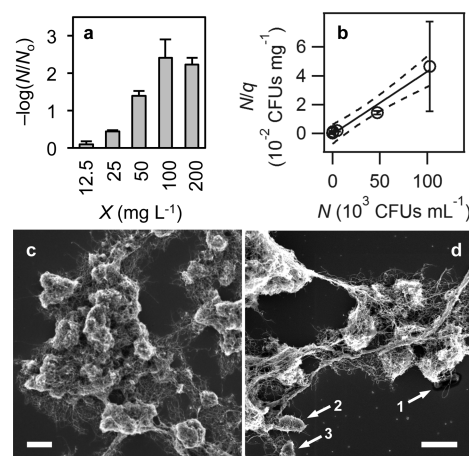

Figure 6. Removal of *E. coli* by carbon nanotube ponytails. (a) Decrease of the number of survived *E. coli.* in the log unit with increasing CNP dosage X. (b) Adsorption isotherm of *E. coli*. The solid line is a least-squares linear regression. Dashed lines are 95% confidence intervals. (c, d) Scanning electron micrographs of CNPs after the adsorption of *E. coli*. Arrows: 1, dehydrated loose cell; 2, wrapped whole cell; 3, wrapped cell fragment. Scale bars: 2 μm.

CNP dosage. As shown in Figure 6b, the removal efficiency conforms to the Langmuir model, suggesting the removal mechanism is sorption. Regression gives a sorption capacity of $q_{max} = 2.3(\pm 0.2) \times 10^9$ CFUs g^{-1} (Table S6, Supporting Information). For each gram of CNPs, there are approximately $4.5(\pm 3.7) \times 10^7$ CNP particles; therefore, each particle captures approximately 50 bacterial cells. If each *E. coli* cell is considered as a sphere with 1 μm diameter, it is plausible for a CNP particle of 120 μm in length to catch more than 50 cells. On the basis of the Langmuir model, for a typical water source containing 10^5 CFUs L^{-1} (of which *E. coli* is often a minute fraction),[61] only 46($\pm$4) mg L^{-1} CNPs is required to achieve 3-log reduction to the commonly acceptable level of 100 CFUs mL^{-1}.[62]

The capturing of bacterial cells by CNPs is further visualized using SEM. As shown in Figure 6c, cells are wrapped tightly by CNP particles as linked aggregates. A careful search over many SEM images reveals three types of cells, as marked in Figure 6d, including (1) dehydrated loose cells (only one found), (2) wrapped whole cell, and (3) wrapped cell fragment. The presence of cell fragments suggests that CNPs are capable of inactivating microorganisms by damaging the cell membrane as other CNTs.[63,64]

In addition to sorption, CNPs also exhibited the ability of catalyzing the reduction of model pollutant *p*-nitrophenol (PNP)[65] in the presence of reducing agent sodium borohydride (NaBH$_4$) (cf. Figure S5, Supporting Information). As shown in Figure 7a, CNP-catalyzed PNP reduction (cyan) follows the pseudo-first-order rate law when NaBH$_4$ is in excess:[66] $\ln(C/C_0) = -kt$, where C and C_0 are residual and initial PNP
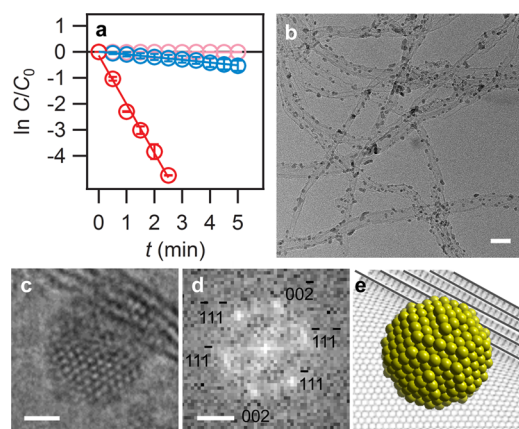
Figure 7. Catalytic reduction of *p*-nitrophenol (PNP) by carbon nanotube ponytails and enhancement of catalytic performance with decoration of palladium (Pd) nanoparticles: Pd-CNPs and PNP with excess sodium borohydride (SB; red), CNPs and PNP with excess SB (cyan), and PNP and SB only (pink). (a) Decrease of PNP concentration C with respect to the initial concentration C_0 with time. (b, c) Transmission electron micrographs of Pd-decorated carbon nanotubes removed from Pd-CNPs by sonication. (d) Fast Fourier transform of part b. (e) A molecular model matching part b. Scale bars: b, 20 nm; c, 1 nm; d, 4 nm^{-1}.

concentrations and k is the reduction rate constant. Linear regression gives $k = 0.26(\pm0.01)$ min^{-1} ($R^2 = 0.99$). Adsorption makes a negligible contribution to the PNP reduction, as evident from the flat line observed in the absence of borohydride (pink). CNPs' catalytic ability can be attributed to the Co nanoparticles in the supporting LDO disc.[67]

To further improve CNPs' catalytic capability, 3 nm palladium (Pd) nanoparticles were decorated on CNPs at a density of $0.25(\pm0.01)$ g-Pd/g-CNP. The 1:4 Pd-to-C mass ratio was confirmed by measurements made with inductively coupled plasma optical emission spectroscopy after acid digestion. As shown in Figure 7b, Pd nanoparticles are uniformly distributed on individual CNTs in CNPs. Figure 7c shows a Pd nanoparticle oriented along the [110] zone axis under TEM. The fast Fourier transform of the TEM image reveals distinctive electron diffractions from (002) and (111) planes, as shown in Figure 7d, suggesting that Pd nanoparticles are single crystalline, which is represented by a truncated octahedral model, as shown in Figure 7e. The presence of Pd nanoparticles has greatly enhanced the reduction of PNP, as shown in Figure 7a (red), with a value of $k = 1.88(\pm0.08)$ min^{-1} ($R^2 = 0.99$). After being normalized to the Pd mass, the value of k gives a rate constant of $608(\pm26)$ L min^{-1} g^{-1}, which is comparable with literature values for Pd-catalyzed PNP reduction.[68−70]

CONCLUSION

In summary, we have demonstrated that individual CNTs can be integrated into micrometer-sized colloidal particles without using a heavy or bulky particulate support. The resulting carbon nanotube ponytails consist of CNTs grown on a nanometer-thin material disc with a negligible mass and volume. Compared to individual CNTs, CNPs can be more effectively separated from water using gravitational sedimentation, magnetic attraction, and membrane filtration while having the ability to perform adsorption, disinfection, and catalytic degradation of contaminants in water. Organizing CNTs into hierarchical

CNPs represents a new strategy to scale up nanomaterials for macroscopic engineering applications. With further development, CNPs can not only be used in treatment processes for water purification but also be deployed to combat accidental spills of chemical and biological contaminants.

METHODS

The materials and methods used to synthesize, characterize, and evaluate materials in this study are described in this section. All chemicals were purchased from Sigma-Aldrich and gases from Airgas unless stated otherwise. More information on the control of CNPs' morphology by varying synthesis parameters can be found in the Supporting Information.

Synthesis of Carbon Nanotube Ponytails. Nitrate salts of aluminum, magnesium, and cobalt were mixed with urea in 100 mL of deionized (DI) water (Millipore). The final concentrations of the precursor ingredients were 100 mmol L^{-1} for urea and 50 mmol L^{-1} for all metals: $\alpha\%$ for Co, $(67 - \alpha)\%$ for Mg, and 33% for Al with α being varied from 5 to 33%. The solution was placed in a sealed autoclave reactor and heated to 100 °C. After a period of time (typically 12 h), layered double hydroxide (LDH) discs were produced. LDH discs were collected by centrifugation, washed with DI water, and calcined at 800 °C in air for 20 min. LDH discs were then placed inside a sealed quartz tubing and heated by a tube furnace to 800 °C under argon protection. Hydrogen was passed through the tubing at 50 sccm for 5 min to reduce LDH to LDO. Ethanol was then supplied by bubbling argon through a reservoir at 100 sccm for 15 min to grow CNT arrays on LDO discs.

Synthesis of Unbounded Carbon Nanotubes. Unbounded CNTs used to compare with CNPs in gravitational settling were prepared using a powder catalyst consisting of cobalt, molybdenum, and magnesium.[39] The growth of CNTs using CVD followed the same procedure as described above except that the powder catalyst was used instead of LDO discs. After 15 min of CVD growth, the powder catalyst was dissolved away by soaking CNTs in concentrated hydrochloric acid at 80 °C for 8 h. The remaining CNTs were cleaned with DI water and freeze-dried (Labconco). The unbounded CNTs have similar morphologies and surface properties as the individual CNTs in CNPs, as described in the Supporting Information.

Preparation and Evaluation of Pd-Decorated CNPs. Nanoparticle decoration was achieved using a one-step protocol[71] by mixing Pd(NO$_3$)$_2$ solution with CNPs. Briefly, 10 mg of CNPs was mixed with 20 mL of DI water in a 50 mL flask under sonication. A 20 mL portion of Pd(NO$_3$)$_2$ solution (5 mM) was added to the flask drop by drop under magnetic stirring. The mixture was permitted to react for 30 min to form PdO nanoparticles on CNPs. PdO-CNPs were collected using an external magnetic field and washed repeatedly with DI water. The washed PdO-CNPs were redispersed in 40 mL of water under sonication. PdO-CNPs were reduced to Pd-CNPs by mixing with sodium borohydride solution. The composition of PdO-CNPs was determined by dissolving the composite in concentrated nitric acid and measuring the Pd content using inductively coupled plasma optical emission spectroscopy (PerkinElmer).

Material Characterization. CNPs and other nanomaterials used in this study were also characterized using a transmission electron microscope (FEI Titan), scanning electron microscope (FEI Magellan 400), powder X-ray diffractometer (Bruker D8 Advance Davinci), X-ray photoelectron spectrometer (PHI 5000 VersaProbe), superconducting quantum interference device (Quantum Design MPMS SQUID), and surface area analyzer (Micromeritics ASAP2020). Sample preparation and analyses were performed following standard procedures.

Gravitational and Magnetic Separation. Gravitational sedimentation was performed in a 1 cm × 1 cm quartz cuvette with a height of 2.5 cm of aqueous suspension. Light passed through a portion of the suspension from the top to 1.3 cm from the bottom. The carbon concentration in suspension was directly quantified by the absorbance of light at 500 nm (Figure S3, Supporting Information). Magnetic separation was performed in a scintillation vial with a

diameter of 2.8 cm using 15 mL of CNP suspension. The block magnet (K&J Magnetics BX0X0C) was placed to the side of the vial. The magnetic field inside the vial has an average strength of 4.2 kOe. To quantify the decrease of CNP concentration with time, 0.1 mL of suspension was taken periodically from the top of the suspension, diluted into 1 mL in a 2 mL quartz cuvette, and measured for light absorbance at 500 nm.

Adsorption of Methylene Blue. Adsorption was quantified by measuring the initial and residual MB concentrations, C_0 and C, using light absorption at 664 nm after an incubation period t under shaking at room temperature.[72] In kinetic studies, 10 mg of CNPs was added in 10 mL of DI water in a glass vial. Solution pH was adjusted with concentrated HCl and NaOH solutions. MB stock solution (1000 ppm) was added to reach a total volume of 15 mL and mixed on a shaking table (300 rmp). Periodically, 0.1 mL of solution was pipetted from the vial, filtered, and measured. After the adsorption experiment, the pH was measured again, which was found to be within 0.3 pH units from the initial pH. In equilibrium studies, 5−10 mg of CNPs was added in 15 mL of aqueous solution containing MB at a predetermined concentration. CNPs and MB were mixed under shaking for 4 h. Solution pH was maintained at a preset value throughout the entire experimental duration using concentrated HCl and NaOH solutions. At the end of the experiment, CNPs were separated from treated water by a magnet and the MB concentrations were measured.

Regeneration of Methylene Blue-Laden Carbon Nanotube Ponytails. A 10 mg portion of CNPs was loaded with an equilibrium amount of MB in a 15 mL aqueous solution with a MB concentration of 120 mg L^{-1} under vigorous shaking for 4 h. CNPs were collected by magnetic separation. To evaluate the effectiveness of ethanol wash, CNPs were added to 15 mL of ethanol under vigorous shaking. To examine the desorption kinetics, 0.1−0.2 mL of solution was taken by pipet periodically to measure the MB concentration in ethanol. The solution was dried in a scintillation vial by evaporating ethanol in a fume hood. The residual MB was redissolved in water for concentration measurement. To examine the efficiency after CNPs were regenerated by 10-cycle ethanol wash, 6 mg of regenerated CNPs was mixed with 15 mL of MB aqueous solution (80 mg L^{-1}) for 4 h. For thermal regeneration by microwave irradiation, CNPs were placed in a scintillation vial inside a kitchen microwave oven (R-209 KK, Sharp Electronics Corp., Mahwan, NJ; 800 W, 2.45 GHz) and the oven was turned on under full power for 3, 5, or 8 min.

Removal of *Escherichia coli*. CNPs' ability to remove pathogenic bacteria was examined using *E. coli* DH5α. The bacterium was first cultivated in the LB liquid medium overnight. The culture was then washed in the phosphate buffered saline (PBS, Invitrogen). The wash was performed by adding 30 μL of the overnight culture into 30 mL of PBS. The washed bacteria were then recollected using a centrifuge as cell pellets. The pellets were resuspended in 30 mL of PBS to simulate contaminated water. CNPs were then added to the simulated water in 4 mL vials. The mixture was first homogenized using a tissue grinder for 20 s and shaken for 1 h. The mixture was then allowed to settle on the bench for 2 h. Water was taken from the top layer for colony forming unit (CFU) counting.

Catalytic Reduction of *p*-Nitrophenol. The reduction of PNP by sodium borohydride (SB) occurs rapidly in the presence of catalysts and can be readily followed using UV/vis spectrometry (Figure S4, Supporting Information).[73] A 0.1 mL portion of well dispersed 0.25 g L^{-1} CNP solution or 0.31 g L^{-1} Pd-decorated CNP solution (same amount of CNPs in both solutions), 1.9 mL of NaBH$_4$ solution, and 0.02 mL of 0.2 mM PNP were mixed in a standard quartz cuvette with a 1 cm path length. The concentration of PNP was monitored every 30 s for 5 min using light absorption at 400 nm. The solution was gently stirred with a glass rod in the catalytic process to avoid catalyst precipitation. An adsorption control experiment was done by replacing NaBH$_4$ solution with 0.0625 mol L^{-1} NaOH solution while keeping the other procedures identical.

ASSOCIATED CONTENT

Ⓢ Supporting Information

Figure S1: Powder X-ray diffraction patterns of layered double hydroxide and layered double oxide discs. Figure S2: Control of physical dimensions of carbon nanotube ponytails (CNPs) by varying synthesis time and cobalt doping. Figure S3: Transmission electron microscopy and X-ray photoelectron spectrum of unbound carbon nanotubes. Figure S4: Visible spectra and the absorbance−concentration relationships for carbon nanotubes and carbon nanotube ponytails dispersed in water. Figure S5: UV/vis spectra of *p*-nitrophenol and *p*-aminophenol and the absorbance−concentration relationship used for *p*-nitrophenol quantification. Tables S1−S6: Results of least-squares regressions in Figures 5 and 6. This material is available free of charge via the Internet at http://pubs.acs.org.

AUTHOR INFORMATION

Corresponding Authors
*E-mail: dingding_an@hms.harvard.edu.
*E-mail: chongzheng.na@gmail.com.

Author Contributions
§These authors contributed equally.

Notes
The authors declare no competing financial interest.

REFERENCES

(1) Rodríguez-Reinoso, F. Activated Carbon and Adsorption. In *Encyclopedia of Materials: Science and Technology*, 2nd ed.; Jürgen Buschow, K. H., Robert, W. C., Merton, C. F., Bernard, I., Edward, J. K., Subhash, M., Patrick, V., Eds.; Elsevier: Oxford, U.K., 2001; pp 22−34.
(2) The Freedonia Group. *World Activated Carbon: Industry Study with Forecasts for 2016 & 2021*; Cleveland, OH, 2012.
(3) Tech Archival. *Global Activated Carbon Market Assessment & Future Opportunities 2008−2018*; Portland, OR, 2013.
(4) Cleaning up Water. *Nat. Mater.* **2008**, 7, 341−341.
(5) Shannon, M. A.; Bohn, P. W.; Elimelech, M.; Georgiadis, J. G.; Marinas, B. J.; Mayes, A. M. Science and Technology for Water Purification in the Coming Decades. *Nature* **2008**, 452, 301−310.
(6) Qu, X. L.; Brame, J.; Li, Q. L.; Alvarez, P. J. J. Nanotechnology for a Safe and Sustainable Water Supply: Enabling Integrated Water Treatment and Reuse. *Acc. Chem. Res.* **2013**, 46, 834−843.
(7) A Fresh Approach to Water. *Nature* **2008**, 452, 253−253.
(8) United Nations World Water Assessment Programme. *The United Nations World Water Development Report 4: Managing Water under Uncertainty and Risk*; Paris, France, 2012.
(9) Iijima, S. Helical Microtubules of Graphitic Carbon. *Nature* **1991**, 354, 56−58.
(10) De Volder, M. F. L.; Tawfick, S. H.; Baughman, R. H.; Hart, A. J. Carbon Nanotubes: Present and Future Commercial Applications. *Science* **2013**, 339, 535−539.
(11) Rao, G. P.; Lu, C.; Su, F. Sorption of Divalent Metal Ions from Aqueous Solution by Carbon Nanotubes: A Review. *Sep. Purif. Technol.* **2007**, 58, 224−231.

(12) Pan, B.; Xing, B. S. Adsorption Mechanisms of Organic Chemicals on Carbon Nanotubes. *Environ. Sci. Technol.* **2008**, *42*, 9005−9013.

(13) Wang, S.; Ng, C. W.; Wang, W.; Li, Q.; Li, L. A Comparative Study on the Adsorption of Acid and Reactive Dyes on Multiwall Carbon Nanotubes in Single and Binary Dye Systems. *J. Chem. Eng. Data* **2012**, *57*, 1563−1569.

(14) Wang, S. B.; Ng, C. W.; Wang, W. T.; Li, Q.; Hao, Z. P. Synergistic and Competitive Adsorption of Organic Dyes on Multiwalled Carbon Nanotubes. *Chem. Eng. J.* **2012**, *197*, 34−40.

(15) Li, Q. L.; Mahendra, S.; Lyon, D. Y.; Brunet, L.; Liga, M. V.; Li, D.; Alvarez, P. J. J. Antimicrobial Nanomaterials for Water Disinfection and Microbial Control: Potential Applications and Implications. *Water Res.* **2008**, *42*, 4591−4602.

(16) Serp, P.; Corrias, M.; Kalck, P. Carbon Nanotubes and Nanofibers in Catalysis. *Appl. Catal., A* **2003**, *253*, 337−358.

(17) Pan, B.; Xing, B. Adsorption Mechanisms of Organic Chemicals on Carbon Nanotubes. *Environ. Sci. Technol.* **2008**, *42*, 9005−9013.

(18) Yang, K.; Wu, W.; Jing, Q.; Zhu, L. Aqueous Adsorption of Aniline, Phenol, and Their Substitutes by Multi-Walled Carbon Nanotubes. *Environ. Sci. Technol.* **2008**, *42*, 7931−7936.

(19) Hameed, B. H.; Din, A. T. M.; Ahmad, A. L. Adsorption of Methylene Blue onto Bamboo-Based Activated Carbon: Kinetics and Equilibrium Studies. *J. Hazard. Mater.* **2007**, *141*, 819−825.

(20) Snoeyink, V. L.; Summers, R. S. Chapter 13: Adsorption of Organic Compounds. In *Water Quality and Treatment: A Handbook of Community Water Supplies*; Letterman, R. L., Ed.; McGraw-Hill: New York, 1999.

(21) Colvin, V. L. The Potential Environmental Impact of Engineered Nanomaterials. *Nat. Biotechnol.* **2003**, *21*, 1166−1170.

(22) Lam, C. W.; James, J. T.; McCluskey, R.; Arepalli, S.; Hunter, R. L. A Review of Carbon Nanotube Toxicity and Assessment of Potential Occupational and Environmental Health Risks. *Crit. Rev. Toxicol.* **2006**, *36*, 189−217.

(23) Aschberger, K.; Johnston, H. J.; Stone, V.; Aitken, R. J.; Hankin, S. M.; Peters, S. A. K.; Tran, C. L.; Christensen, F. M. Review of Carbon Nanotubes Toxicity and Exposure-Appraisal of Human Health Risk Assessment Based on Open Literature. *Crit. Rev. Toxicol.* **2010**, *40*, 759−790.

(24) Lowry, G. V.; Hotze, E. M.; Bernhardt, E. S.; Dionysiou, D. D.; Pedersen, J. A.; Wiesner, M. R.; Xing, B. S. Environmental Occurrences, Behavior, Fate, and Ecological Effects of Nanomaterials: An Introduction to the Special Series. *J. Environ. Qual.* **2010**, *39*, 1867−1874.

(25) Lee, J.; Mahendra, S.; Alvarez, P. J. J. Nanomaterials in the Construction Industry: A Review of Their Applications and Environmental Health and Safety Considerations. *ACS Nano* **2010**, *4*, 3580−3590.

(26) He, D.; Bozlar, M.; Genestoux, M.; Bai, J. Diameter- and Length-Dependent Self-Organizations of Multi-Walled Carbon Nanotubes on Spherical Alumina Microparticles. *Carbon* **2010**, *48*, 1159−1170.

(27) Kim, D. Y.; Sugime, H.; Hasegawa, K.; Osawa, T.; Noda, S. Sub-Millimeter-Long Carbon Nanotubes Repeatedly Grown on and Separated from Ceramic Beads in a Single Fluidized Bed Reactor. *Carbon* **2011**, *49*, 1972−1979.

(28) Kim, D. Y.; Sugime, H.; Hasegawa, K.; Osawa, T.; Noda, S. Fluidized-Bed Synthesis of Sub-Millimeter-Long Single Walled Carbon Nanotube Arrays. *Carbon* **2012**, *50*, 1538−1545.

(29) Li, W.; Yuan, J.; Lin, Y.; Yao, S.; Ren, Z.; Wang, H.; Wang, M.; Bai, J. The Controlled Formation of Hybrid Structures of Multi-Walled Carbon Nanotubes on Sic Plate-Like Particles and Their Synergetic Effect as a Filler in Poly(Vinylidene Fluoride) Based Composites. *Carbon* **2013**, *51*, 355−364.

(30) Yan, H.; Gong, A. J.; He, H. S.; Zhou, J.; Wei, Y. X.; Lv, L. Adsorption of Microcystins by Carbon Nanotubes. *Chemosphere* **2006**, *62*, 142−148.

(31) El-Sheikh, A. H.; Sweileh, J. A.; Al-Degs, Y. S.; Insisi, A. A.; Al-Rabady, N. Critical Evaluation and Comparison of Enrichment

Efficiency of Multi-Walled Carbon Nanotubes, C18 Silica and Activated Carbon Towards Some Pesticides from Environmental Waters. *Talanta* **2008**, *74*, 1675−1680.

(32) Li, F.; Tan, Q.; Evans, D. G.; Duan, X. Synthesis of Carbon Nanotubes Using a Novel Catalyst Derived from Hydrotalcite-Like Co-Al Layered Double Hydroxide Precursor. *Catal. Lett.* **2005**, *99*, 151−156.

(33) Zhao, Y.; Jiao, Q. Z.; Li, C. H.; Liang, J. Catalytic Synthesis of Carbon Nanostructures Using Layered Double Hydroxides as Catalyst Precursors. *Carbon* **2007**, *45*, 2159−2163.

(34) Zhao, M.-Q.; Zhang, Q.; Zhang, W.; Huang, J.-Q.; Zhang, Y.; Su, D. S.; Wei, F. Embedded High Density Metal Nanoparticles with Extraordinary Thermal Stability Derived from Guest−Host Mediated Layered Double Hydroxides. *J. Am. Chem. Soc.* **2010**, *132*, 14739−14741.

(35) Zhao, M.-Q.; Peng, H.-J.; Zhang, Q.; Huang, J.-Q.; Tian, G.-L.; Tang, C.; Hu, L.; Jiang, H.-R.; Cai, H.-Y.; Yuan, H.-X.; Wei, F. Controllable Bulk Growth of Few-Layer Graphene/Single-Walled Carbon Nanotube Hybrids Containing Fe@C Nanoparticles in a Fluidized Bed Reactor. *Carbon* **2014**, *67*, 554−563.

(36) Vix-Guterl, C.; Couzi, M.; Dentzer, J.; Trinquecoste, M.; Delhaes, P. Surface Characterizations of Carbon Multiwall Nanotubes: Comparison between Surface Active Sites and Raman Spectroscopy. *J. Phys. Chem. B* **2004**, *108*, 19361−19367.

(37) Delhaes, P.; Couzi, M.; Trinquecoste, M.; Dentzer, J.; Hamidou, H.; Vix-Guterl, C. A Comparison between Raman Spectroscopy and Surface Characterizations of Multiwall Carbon Nanotubes. *Carbon* **2006**, *44*, 3005−3013.

(38) Jiang, H.; Zhu, L.; Moon, K. S.; Wong, C. P. The Preparation of Stable Metal Nanoparticles on Carbon Nanotubes Whose Surfaces Were Modified During Production. *Carbon* **2007**, *45*, 655−661.

(39) Wang, H.; Lin, K.; Jing, B.; Krylova, G.; Sigmon, G. E.; McGinn, P.; Zhu, Y.; Na, C. Removal of Oil Droplets from Contaminated Water Using Magnetic Carbon Nanotubes. *Water Res.* **2013**, *47*, 4198−4205.

(40) Adamson, A. W. *Physical Chemistry of Surfaces*; John Wiley & Sons: New York, 1990.

(41) Brunauer, S.; Emmett, P. H.; Teller, E. Adsorption of Gases in Multimolecular Layers. *J. Am. Chem. Soc.* **1938**, *60*, 309−319.

(42) Chiodarelli, N.; Richard, O.; Bender, H.; Heyns, M.; De Gendt, S.; Groeseneken, G.; Vereecken, P. M. Correlation between Number of Walls and Diameter in Multiwall Carbon Nanotubes Grown by Chemical Vapor Deposition. *Carbon* **2012**, *50*, 1748−1752.

(43) Laurent, C.; Flahaut, E.; Peigney, A. The Weight and Density of Carbon Nanotubes Versus the Number of Walls and Diameter. *Carbon* **2010**, *48*, 2994−2996.

(44) Gregory, R.; Zabel, T. F.; Edzwald, J. K. Chapter 11: Sedimentation and Flotation. In *Water Quality and Treatment: A Handbook of Community Water Supplies*; Letterman, R. L., Ed.; McGraw-Hill: New York, 1999.

(45) Farley, K. J.; Morel, F. M. M. Role of Coagulation in the Kinetics of Sedimentation. *Environ. Sci. Technol.* **1986**, *20*, 187−195.

(46) Lick, W. *Sediment and Contaminant Transport in Surface Waters*; CRC Press: Boca Raton, FL, 2008.

(47) Tanaka, T. Filtration Characteristics of Carbon Nanotubes and Preparation of Buckypapers. *Desalin. Water Treat.* **2010**, *17*, 193−198.

(48) Carman, P. C. Fluid Flow through Granular Beds. *Chem. Eng. Res. Des.* **1997**, *75*, S32−S48.

(49) Gong, J. L.; Wang, B.; Zeng, G. M.; Yang, C. P.; Niu, C. G.; Niu, Q. Y.; Zhou, W. J.; Liang, Y. Removal of Cationic Dyes from Aqueous Solution Using Magnetic Multi-Wall Carbon Nanotube Nanocomposite as Adsorbent. *J. Hazard. Mater.* **2009**, *164*, 1517−1522.

(50) Yao, Y. J.; Xu, F. F.; Chen, M.; Xu, Z. X.; Zhu, Z. W. Adsorption Behavior of Methylene Blue on Carbon Nanotubes. *Bioresour. Technol.* **2010**, *101*, 3040−3046.

(51) Liu, Y.; Shen, L. From Langmuir Kinetics to First- and Second-Order Rate Equations for Adsorption. *Langmuir* **2008**, *24*, 11625−11630.

(52) Chagovets, V. V.; Kosevich, M. V.; Stepanian, S. G.; Boryak, O. A.; Shelkovsky, V. S.; Orlov, V. V.; Leontiev, V. S.; Pokrovskiy, V. A.;

Adamowicz, L.; Karachevtsev, V. A. Noncovalent Interaction of Methylene Blue with Carbon Nanotubes: Theoretical and Mass Spectrometry Characterization. *J. Phys. Chem. C* **2012**, *116*, 20579−20590.

(53) Hiemenz, P. C.; Rajagopalan, R. *Principles of Colloid and Surface Chemistry*, 3rd ed.; Marcel Dekker: New York, 1997.

(54) Hahner, G.; Marti, A.; Spencer, N. D.; Caseri, W. R. Orientation and Electronic Structure of Methylene Blue on Mica: A near Edge X-Ray Absorption Fine Structure Spectroscopy Study. *J. Chem. Phys.* **1996**, *104*, 7749−7757.

(55) Hang, P. T. Methylene Blue Absorption by Clay Minerals: Determination of Surface Areas and Cation Exchange Capacities (Clay-Organic Studies XVIII). *Clays Clay Miner.* **1970**, *18*, 203−212.

(56) Kahr, G.; Madsen, F. T. Determination of the Cation Exchange Capacity and the Surface Area of Bentonite, Illite and Kaolinite by Methylene Blue Adsorption. *Appl. Clay Sci.* **1995**, *9*, 327−336.

(57) He, X.; Male, K. B.; Nesterenko, P. N.; Brabazon, D.; Paull, B.; Luong, J. H. T. Adsorption and Desorption of Methylene Blue on Porous Carbon Monoliths and Nanocrystalline Cellulose. *ACS Appl. Mater. Interfaces* **2013**, *5*, 8796−8804.

(58) Ai, L. H.; Jiang, J. Removal of Methylene Blue from Aqueous Solution with Self-Assembled Cylindrical Graphene-Carbon Nanotube Hybrid. *Chem. Eng. J.* **2012**, *192*, 156−163.

(59) Yuen, F. K.; Hameed, B. H. Recent Developments in the Preparation and Regeneration of Activated Carbons by Microwaves. *Adv. Colloid Interface Sci.* **2009**, *149*, 19−27.

(60) Na, C.; Olson, T. M. Mechanism and kinetics of cyanogen chloride formation from the chlorination of glycine. *Environ. Sci. Technol.* **2006**, *40*, 1469−1477.

(61) Hoefel, D.; Grooby, W. L.; Monis, P. T.; Andrews, S.; Saint, C. P. Enumeration of Water-Borne Bacteria Using Viability Assays and Flow Cytometry: A Comparison to Culture-Based Techniques. *J. Microbiol. Methods* **2003**, *55*, 585−597.

(62) Bartram, J.; Cotruvo, J.; Exner, M.; Fricker, C.; Glasmacher, A. *Heterotrophic Plate Counts and Drinking-Water Safety: The Significance of Hpcs for Water Quality and Human Health*; IWA Publishing on behalf of the World Health Organization: London, 2003.

(63) Kang, S.; Herzberg, M.; Rodrigues, D. F.; Elimelech, M. Antibacterial Effects of Carbon Nanotubes: Size Does Matter! *Langmuir* **2008**, *24*, 6409−6413.

(64) Arias, L. R.; Yang, L. Inactivation of Bacterial Pathogens by Carbon Nanotubes in Suspensions. *Langmuir* **2009**, *25*, 3003−3012.

(65) United States Environmental Protection Agency, Clean Water Act Priority Pollutant List. 1982; p Code of Federal Regulations 40 CFR 423 Appendix A.

(66) Hong, X. J.; Fan, X. A.; Wu, Z. Y.; Wang, G. Q.; Zhu, C. Y.; Li, G. Q.; Hou, Y. H., Preparation and Microstructure Control of One-Dimension Core-Shell Heterostructure of Te/Bi, Te/Bi$_2$te$_3$ by Microwave Assisted Chemical Synthesis. In *Energy and Environment Materials*; Tang, X. F., Wu, Y., Yao, Y., Zhang, Z. Z., Eds.; Trans Tech Publications Inc.: Dürnten, Switzerland, 2013; pp 153−160.

(67) Sahiner, N.; Ozay, H.; Ozay, O.; Aktas, N. A Soft Hydrogel Reactor for Cobalt Nanoparticle Preparation and Use in the Reduction of Nitrophenols. *Appl. Catal., B* **2010**, *101*, 137−143.

(68) Bhandari, R.; Knecht, M. R. Effects of the Material Structure on the Catalytic Activity of Peptide-Templated Pd Nanomaterials. *ACS Catal.* **2011**, *1*, 89−98.

(69) Harish, S.; Mathiyarasu, J.; Phani, K.; Yegnaraman, V. Synthesis of Conducting Polymer Supported Pd Nanoparticles in Aqueous Medium and Catalytic Activity Towards 4-Nitrophenol Reduction. *Catal. Lett.* **2009**, *128*, 197−202.

(70) Mei, Y.; Lu, Y.; Polzer, F.; Ballauff, M.; Drechsler, M. Catalytic Activity of Palladium Nanoparticles Encapsulated in Spherical Polyelectrolyte Brushes and Core-Shell Microgels. *Chem. Mater.* **2007**, *19*, 1062−1069.

(71) He, H. K.; Gao, C. A General Strategy for the Preparation of Carbon Nanotubes and Graphene Oxide Decorated with PdO Nanoparticles in Water. *Molecules* **2010**, *15*, 4679−4694.

(72) Bergmann, K.; Okonski, C. T. A Spectroscopic Study of Methylene Blue Monomer, Dimer, and Complexes with Montmorillonite. *J. Phys. Chem.* **1963**, *67*, 2169−2177.

(73) Pradhan, N.; Pal, A.; Pal, T. Catalytic Reduction of Aromatic Nitro Compounds by Coinage Metal Nanoparticles. *Langmuir* **2001**, *17*, 1800−1802.

9434

dx.doi.org/10.1021/am501810f | *ACS Appl. Mater. Interfaces* 2014, 6, 9426−9434